JACS
JOURNAL OF THE AMERICAN CHEMICAL SOCIETY
Article
pubs.acs.org/JACS

Dopant-Controlled Selenization in Pd Nanocrystals: The Triggered Kirkendall Effect

Amit K. Guria, Gyanaranjan Prusty, Biplab K. Patra, and Narayan Pradhan*

Department of Materials Science and Center for Advanced Materials, Indian Association for the Cultivation of Science, Kolkata, India 700032

Supporting Information

ABSTRACT: Doping foreign impurities in host nanomaterials can induce new materials properties. In addition, doping can also influence the crystallization process and change the shape and/or phase of the host material. While dopant-induced changes in the properties of materials have been well studied, the concept of doping and its chemistry in the design of different nanostructures has rarely been investigated. In order to further understand the doping chemistry, this study investigated the dopant-controlled enhancement of the rate of the chemical reaction during the transformation from one doped material to another and the consequent effect on the shape evolution of the nanostructures. These are performed during the selenization of metal Pd(0), using Ag dopant. While the controlled process produced cuboidal $Pd_{17}Se_{15}$ from the quasi-spherical nanocrystals of Pd(0), on doping, the shape of $Pd_{17}Se_{15}$ transformed into hollow cubes. The rate was also enhanced by more than 30 times for the doped case in comparison to undoped Pd(0). Importantly, while for the undoped nanocrystals, the selenization approached in one direction, where for the doped particles, it occurred all around the nanocrystals and triggered the Kirkendall effect. Detailed investigations were conducted to elucidate the influence of the dopant on both the rate and directional approach of selenization in Pd(0), initiation of the fast diffusion of Pd, change in shape, and formation of the hollow structures. To our understanding, the role of dopants in controlling chemical processes is of fundamental importance, and this will undoubtedly broaden the scope of research on the chemistry of doping and crystal growth in solution.

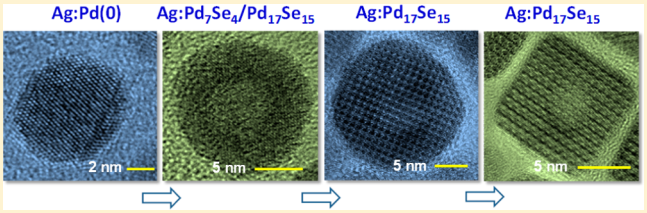

INTRODUCTION

Doping, the process of inserting impurity atoms into a host lattice, can influence the existing properties of the host material.[1−13] Hence, doping has recently been used as a new method to generate functional materials that are required to meet current technological needs. Many studies have been conducted on the doping of a wide variety of inorganic dopants into various metal oxide and semiconductor host nanomaterials, and the properties of the newly formed materials have been well studied.[1−9,14−27] Optically active dopants can create new electronic states and can assist in the creation of new optical centers to produce different colored emissions.[1−8,14−17,28−30] Similarly, magnetic dopants can even introduce magnetic properties in nonmagnetic hosts.[9,18−22] Recently, it has been reported that dopants can influence the charge carrier density of the host materials and thus generate metallic-type localized surface plasmon resonance in semiconductor nanostructures.[23−27]

Apart from influencing the properties of materials, dopants can also interfere with the ongoing crystal growth process and assist the formation of the structural architecture of various nanoscale materials.[31−39] Through adsorption onto the growth facets, dopants can slow down or even stop the directional growth of the nanomaterials, and they can also change the phase as well as shape of some nanostructures.[31−36] It is also reported that the shape of the host nanostructures can be tuned depending on the dopant percentage.[32] However, studies on the influence of dopants on the changes in the crystal growth are very limited, and the fundamental aspects of such growths, which typically do not follow classical growth mechanisms, have not yet been widely explored. Furthermore, most of the successful studies that have been conducted to understand the concept of doping, dopant adsorption or insertion, the doping process, and the change in the properties or shape of materials are associated with the physical processes related to the crystal design or the changes in the physical properties of the nanostructures. However, the use of dopants to control the directional approach or rate of the chemical processes, where the chemical changes govern the shape architecture, has not yet been studied. We explored here both the dopant-induced enhancement of the rate of the chemical reaction and the change in the approach of the chemical transformation during the selenization process that transforms the doped metal (0) into doped metal selenide nanostructures. The process not only induces a chemical reaction but also triggers the Kirkendall effect that transforms the metal selenides to hollow nanostructures. This study has been performed in metal Pd(0) with Ag as dopant for the formation of doped palladium selenide, $Ag:Pd_{17}Se_{15}$. On selenization, the undoped quasi-

Received: February 1, 2015
Published: March 31, 2015

DOI: 10.1021/jacs.5b01103
J. Am. Chem. Soc. 2015, 137, 5123−5129

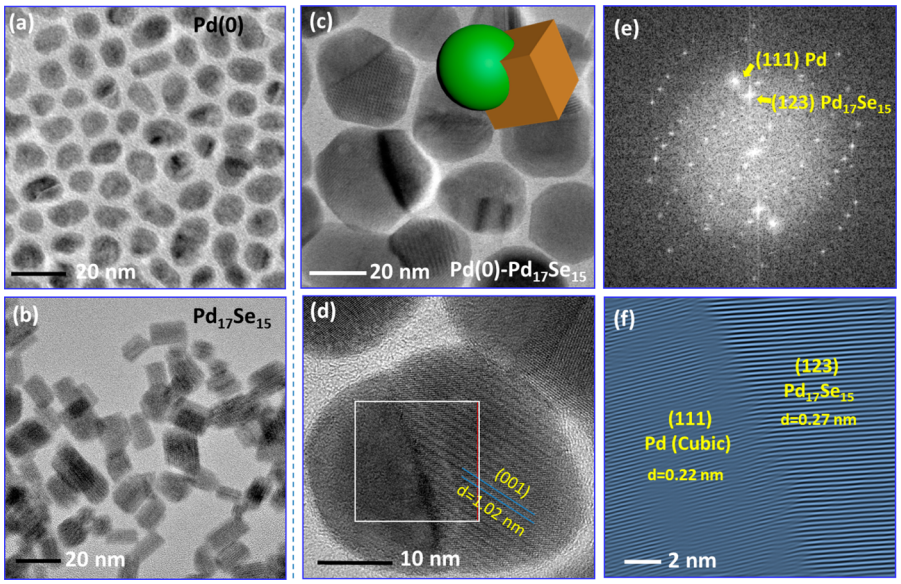

Figure 1. TEM image of (a) Pd(0) nanocrystals and (b) the $Pd_{17}Se_{15}$ cuboid nanostructures. (c) Magnified TEM image of the intermediate heterostructures. (d) HRTEM image of a single heterostructure. (e) Selected area FFT (marked in panel d) at the heterojunction. (f) Simulated HRTEM image with one of the {111} planes of fcc Pd and one of the {123} planes of $Pd_{17}Se_{15}$.

spherical metal particles of Pd(0) while proceed with unidirectional approach for the transformation into $Pd_{17}Se_{15}$, the doped Pd(0) nanocrystals lead to hollow nanocubes of $Pd_{17}Se_{15}$ following all directions Se approach. The selenization rate has also been enhanced more than 30 times faster in doped metal nanocrystals, which initiated the faster diffusion of Pd atoms from the core and triggered the Kirkendall effect. Thorough investigation of the dopant-induced chemical transformation during the selenization process was conducted, the sequential change in the compositions during the transformation from Pd(0) to $Pd_{17}Se_{15}$ was established, and the dopant-induced Kirkendall effect was studied.

EXPERIMENTAL SECTION

Materials. Palladium(II) acetylacetonate ($Pd(acac)_2$, 99%), silver chloride (AgCl, 99.999%), Se powder (99.5%), hexadecylamine (HDA, tech, 90%), and trioctylphosphine oxide (TOPO, tech, 90%) were purchased from Aldrich. All the chemicals were used without further purification.

Synthesis of Nanocrystals. *Synthesis of $Pd_{17}Se_{15}$ Cuboids.* Cuboidal palladium selenide nanocrystals were synthesized by mixing a selenium precursor with palladium nanocrystals. In a typical experiment, a mixture of 0.2 mmol (61 mg) $Pd(acac)_2$ and 4 g HDA was loaded into a three-necked flask and degassed at a temperature of 60 °C for 15 min by purging N_2 gas. Subsequently, the temperature was increased to 280 °C. The solution was maintained at this temperature for 10 min in order to obtain Pd(0) nanocrystals.

In a separate three-necked flask, 0.8 mmol Se powder (63 mg), 1.2 g TOPO, and 4 g of HDA were mixed and subsequently degassed at a temperature of 60 °C for 15 min. It was then heated to a temperature of 270 °C. The Pd(0) reaction mixture was hot injected into this reaction flask and annealed for 45 min at a temperature of 260 °C. The reaction mixture was subsequently collected in a syringe and injected into a centrifuge tube containing hot (60 °C) ethanol. Subsequently, the nanocrystals were precipitated by centrifugation and purified twice using the ethanol-acetone mixture.

Synthesis of Ag-Doped $Pd_{17}Se_{15}$ Hollow Cubes. The Ag:$Pd_{17}Se_{15}$ nanocubes were synthesized using AgCl (2−10 mol % to $Pd(acac)_2$). In a typical process, 2.9 mg (0.02 mmol) of AgCl (10%), 61 mg (0.2 mmol) of $Pd(acac)_2$, and 4 g of HDA were taken in a three necked flask. The mixture was degassed at 60 °C for 15 min by purging N_2 gas, and the temperature was subsequently increased to 280 °C. The rest of the procedure was same as written for $Pd_{17}Se_{15}$ cuboids.

Characterization. The X-ray diffraction (XRD) analysis of the nanocrystals was performed using a Bruker D8 Advance powder diffractometer, using Cu K_α (λ= 1.54 Å) as the incident radiation. Transmission electron microscopy (TEM), high-resolution TEM (HR-TEM), and high-angle annular dark-field scanning transmission electron microscopy (HAADF-STEM) images were captured on a UHR FEG-TEM, JEOL JEM-2100F electron microscope using a 200 kV electron source. The specimens were prepared by dropping a drop of nanocrystal solution in chloroform onto a carbon coated copper grid, and the grid was subsequently dried under ambient conditions. The composition of the nanocrystal was determined by ICP-AES using a PerkinElmer Optima 2100 DV Instrument. The doped nanocrystals were initially repeatedly purified to remove excess precursors. Subsequently, the purified nanocrystals were dissolved in chloroform. The chloroform was subsequently evaporated, and the dried nanocrystals were digested in concentrated HNO_3. The nitric acid solution of the samples was diluted with double-distilled water in order to perform the measurements.

RESULTS AND DISCUSSION

Unidirectional Selenization Approach in Pd(0) Nanocrystals. In order to perform selenization on the Pd(0) nanocrystals, we adopted an in situ conversion process to transform Pd(0) into Pd(II) in the presence of selenium. By heating the Pd precursor (palladium(II) acetylacetonate) in alkyl amine, quasi-spherical particles of Pd(0) were formed. On mixing this solution with Se powder dissolved in alkylamine and alkylphosphine oxide, these quasi-spherical Pd(0) nanocrystals transformed into a cuboidal $Pd_{17}Se_{15}$ semiconductor nanostructure. The stoichiometric composition of palladium selenide was confirmed by powder XRD analysis and selected area fast Fourier transform (FFT) analysis (which will be discussed in a following section). Figure 1a,b presents the TEM images of the initial Pd(0) nanocrystals and the cuboid $Pd_{17}Se_{15}$ nanostructures that were obtained from a typical reaction, respectively. The average diameter of the nanocrystals remained at 10 nm, and the average length and width of the cuboids remained at 15 and 10 nm, respectively.

DOI: 10.1021/jacs.5b01103
J. Am. Chem. Soc. 2015, 137, 5123−5129

To follow this selenization approach, we collected samples at the intermediate stage of the reaction. Interestingly, this exhibited the heterodimers of the Pd(0) and $Pd_{17}Se_{15}$ nanostructures (Figure 1c,d). This clearly suggests that the cuboid shapes of $Pd_{17}Se_{15}$ originated from the Pd(0) and that the selenization process was favored on one specific facet of Pd(0). Figure 1d indicates that two different contrasts can be observed in the HRTEM image of the heterodimers; the darker contrast can be attributed to Pd(0), and the lighter one is from the $Pd_{17}Se_{15}$. Both the elemental mapping and the line scan of a single heterostructure also suggested that a junction formed by the Pd and $Pd_{17}Se_{15}$ nanostructures (Figure S1). An epitaxy was also observed at the heterojunction of these two materials. The selected area FFT pattern obtained from Figure 1d is shown in Figure 1e. From the calculated *d*-spacings and plane angles, it can be concluded that the $Pd_{17}Se_{15}$ exhibits a primitive cubic phase. The two bright spots (marked) on the FFT pattern suggest that an epitaxy is formed between the {111} planes of fcc Pd and the {123} planes of cubic $Pd_{17}Se_{15}$. Hence, the selenization was favored here on one of the {111} facets of Pd(0). The simulated HRTEM image corresponding to these spots is presented in Figure 1f, and the *d*-spacings are marked according to the respective planes of both counterparts.

To further characterize these nanostructures, we conducted powder XRD analysis on the samples that were collected during the different stages of the reaction (Figure 2). From the XRD

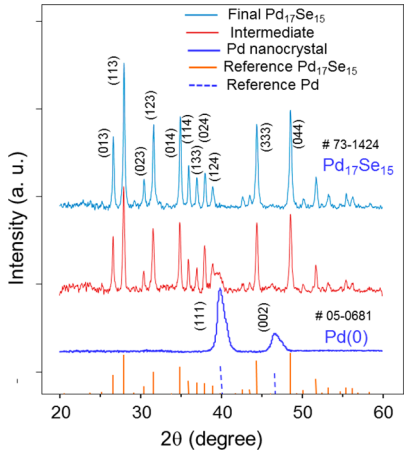

Figure 2. Powder XRD patterns of the Pd(0), intermediate Pd–$Pd_{17}Se_{15}$ heterostructure, and cuboidal $Pd_{17}Se_{15}$.

patterns, it can be observed that Pd(0) is formed in a face-centered cubic phase (PDF no. 05-0681) and that $Pd_{17}Se_{15}$ is formed in a primitive cubic phase (PDF no. 73-1424); these results are also confirmed by the HRTEM analysis. The XRD pattern of the intermediate heterodimers retains the peaks of both the Pd(0) and $Pd_{17}Se_{15}$ phases (Figure 2). This further suggests that during the selenization process, the cubic Pd(0) nanocrystals are directly transformed into cubic $Pd_{17}Se_{15}$ nanostructures without any other intermediate phase. This mechanism for the formation of the nanostructures with an intermediate heterostructure has previously been reported.[40]

The Selenization Approach on Doped Metal and Formation of Hollow Nanocubes. To investigate the effect of the dopants, we introduced Ag during the initiation of the formation of the Pd(0) nanocrystals. As a result of the similar sizes of the Pd and Ag atoms (atomic radii of Pd and Ag are 169 and 165 pm, respectively), the Ag is comfortably accommodated in the fcc Pd(0) lattice. It was also established that the alloy formation of Ag and Pd is thermodynamically favorable.[41,42] We also observed the alloy formation by introducing more Ag (40%) into the reaction system. The peak positions in the powder XRD patterns demonstrate a shift that is similar to that observed during the formation of an alloy (Figure S2). However, we only introduced a small amount of the Ag atoms to study the selenization of the Pd–Ag system.[43] In addition, the presence of excess Ag (~20% or more) allowed the reaction to proceed faster and led to the production of undesirable products (Figure S3). Hence, here we refer the Ag as dopant and for the synthesis of the Ag doped Pd(0) nanocrystals, not more than 10% of Ag in comparison to the Pd-precursor was used for carrying out different reactions.

Figures 3a and S4a show the TEM images of the Ag doped Pd(0) nanocrystals which were obtained using 10% AgCl.

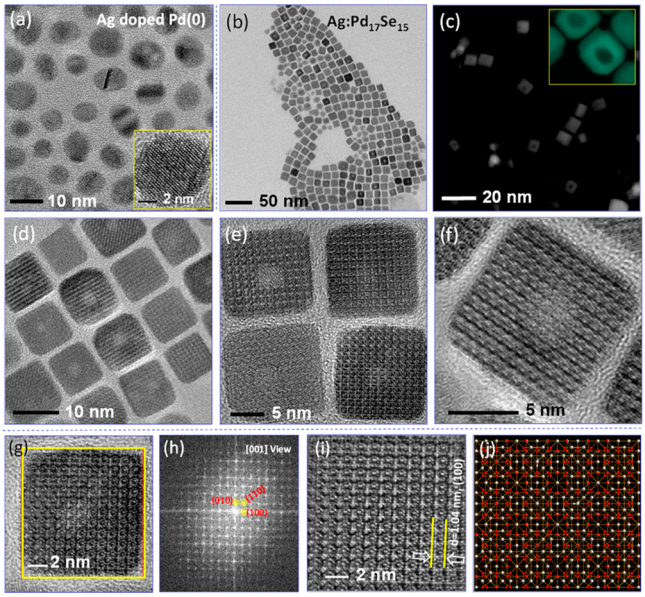

Figure 3. (a) TEM image of Ag doped Pd(0) nanocrystals. Inset is the HRTEM image of a single doped metal particle. (b) TEM and (c) HAADF-STEM images of Ag doped $Pd_{17}Se_{15}$ nanocubes. The inset is a magnified view. (d–f) HRTEM images of doped $Pd_{17}Se_{15}$ nanocubes. (g) Typical HRTEM image of single nanocube, (h) selected area (in g) FFT, (i) simulated HRTEM from the FFT pattern and (j) a ball and stick atomic model of $Pd_{17}Se_{15}$ viewed along the [001] direction. White balls reflect Pd atoms and red for Se.

These particles retained the same shape as that of the undoped Pd(0). The powder XRD analysis results obtained from these doped nanocrystals also retained (Figure S4b) all the peaks in same positions as in undoped Pd(0). However, both the ICP-AES (Table S1) and EDAX data (Figure S5) suggest that Ag is retained within the nanocrystals and its atomic percentage remains at 9.5%, in comparison to the Pd. These results suggested that the small amount of Ag that was used during this study did not alter the shape or phase of the doped metal nanostructures.

However, contrasting results were obtained when these doped Pd(0) nanostructures were treated for selenization using a similar method to that followed for the undoped metal. It was observed that hollow cubic-shaped Ag doped $Pd_{17}Se_{15}$ nanostructures were formed instead of the cuboid shape. Figures 3b and S6 exhibit the TEM images of a typical sample (using 10% AgCl) obtained on selenization, following 30 min

DOI: 10.1021/jacs.5b01103
J. Am. Chem. Soc. 2015, 137, 5123–5129

of annealing. In the majority of cases, these nanocubes exhibit contrasting differences between their cores and edges. The HAADF-STEM image presented in Figure 3c is clearly indicating that these structures are hollow. A magnified image is depicted in the inset, where the hollow space is prominently visible. The HRTEM images of these cubes are also presented in Figure 3d–f, which further imply that these structures are both hollow and crystalline. The *d*-spacing of 1.04 nm reflects the {100} planes of $Pd_{17}Se_{15}$. For a more thorough illustration, the HRTEM image of another hollow cube, a selected area FFT pattern, the simulated HRTEM analysis, and an atomic model of $Pd_{17}Se_{15}$ are shown in Figure 3(g–j), respectively. When comparing the HRTEM and simulated HRTEM images, it can be further observed that the poor contrast at the center of the HRTEM image is not clearly visible in the simulated image; this suggests that the hollow space remains at the core and may not be exposed to the surface. The powder XRD pattern of this final sample (discussed later) indicates that the crystal phase remained the same as that of the undoped $Pd_{17}Se_{15}$. The EDAX data (Figure S5) show that these doped hollow structures retain the Ag in a similar manner to the doped Pd(0). The ICP-AES data also support the Pd to Ag atomic ratio as 9.41 (Table S1). Hence, it can be speculated that following selenization of the doped metal, the shape changes, but the phase of the final structure is the same as that of the undoped structure.

Further, to understand the directional approach of the selenization process, we collected intermediate samples during different stages of the reaction, and these were analyzed microscopically. Figure 4 shows the TEM images of the

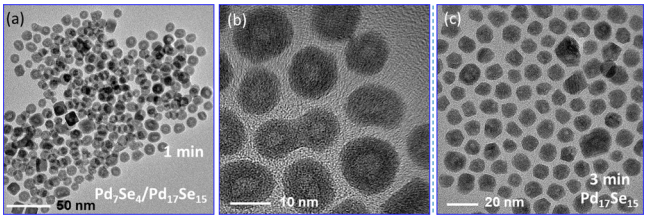

Figure 4. (a) TEM image and (b) magnified TEM image of the samples obtained following a period of 1 min of the selenization process, and (c) TEM image of the sample taken following a period of 3 min of the selenization process, during the transformation from Pd(0) to $Pd_{17}Se_{15}$.

samples obtained at a period of 1 and 3 min following the selenization of doped Pd nanocrystals obtained using 10% AgCl. Close analysis of these images indicates that the hollow structures are formed within a small time frame during the reaction, though these structures still retain a quasi-spherical shape similar to that of the doped metal (0) (Figure 3a). However, the image of the sample collected at 3 min indicates that following the formation of the hollow structure, surface reconstruction occurred before its transformation into a cubic shape. This suggests that the shape change follows the chemical transformation in two steps: the formation of the hollow structure and the shape reconstruction. To further understand the chemistry of these changes, we successively investigated both these processes.

The Dopant-Induced Kirkendall Effect. To understand the mechanism for the formation of the hollow structures, which can even be observed within a period of 1 min following the Se precursor mixing, we analyzed both the powder XRD pattern and the HRTEM images of the collected intermediate sample; this was compared with the 30 min annealed sample. Figure 5 shows the XRD patterns for the samples that were

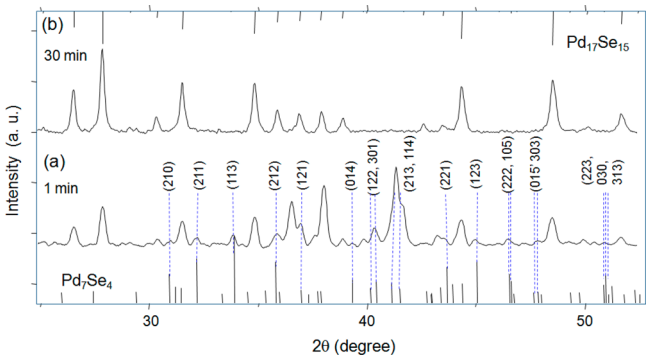

Figure 5. Powder XRD patterns of the sample collected after (a) 1 and (b) 30 min of the selenization reaction. Sample (a) contains the mixture of Pd_7Se_4 and $Pd_{17}Se_{15}$, while the final sample only contains $Pd_{17}Se_{15}$. The standards for Pd_7Se_4 orthorhombic phase (PDF no. 43-0856) and $Pd_{17}Se_{15}$ cubic phase (PDF no. 73-1424) are shown at the bottom and top, respectively.

annealed for 1 and 30 min; for comparison, the standard peaks are also provided at the bottom and top of the panel. Interestingly, it can be observed that the peaks of the final samples overlap with the peaks of the cubic $Pd_{17}Se_{15}$. However, the early stage sample contains some additional peaks. During the analysis, it was observed that these peaks generally resemble the peaks of the bulk orthorhombic Pd_7Se_4 (PDF no. 43-0856). This suggests that the selenization process for the doped Pd(0) proceeds progressively and that the composition changes before the formation of the doped $Pd_{17}Se_{15}$ hollow cube. However, interestingly, these additional peaks are even absent in the XRD pattern of the sample that was subjected to the selenization process for 3 min, suggesting that the conversion from Pd(0) to $Pd_{17}Se_{15}$ is fast and that the final phase does not control the final shape of the nanostructures. The peak intensity of both the compositions in the sample subjected to the selenization process for 1 min also suggests that the percentage of $Pd_{17}Se_{15}$ is much higher than that of Pd_7Se_4. This observation is contrary to the selenization of the undoped Pd(0) which proceeds at a much slower rate and exhibits a direct phase transition from cubic Pd(0) to cubic $Pd_{17}Se_{15}$. However, as palladium selenide can exist with a different stoichiometry,[44−48] this progressive transition for the doped sample is highly possible. To confirm this, we further analyzed the HRTEM images obtained from this intermediate samples.

Figure 6a shows the HRTEM image of an intermediate single hollow nanocrystal. The differences in the contrasts of this image clearly suggest that there is some empty space at the core. However, to understand the possible existence of multiple compositions of palladium selenide, we obtained FFTs from different positions. Figure 6b,c presents the FFT patterns obtained from the entire area (marked 1) and from the side of a nanocrystal (marked 2), respectively (for details, see figure caption). Interestingly, it can be observed that the FFT pattern obtained from the side of the nanocrystal is different to that obtained from the center. The FFT pattern of entire area actually represents the mixture of the patterns of the core and of the side of the nanocrystal. To understand more about their origins, we isolated the FFTs (Figure 6d,g) and simulated the HRTEM. Intriguingly, the simulated HRTEM images (Figure

DOI: 10.1021/jacs.5b01103
J. Am. Chem. Soc. 2015, 137, 5123−5129

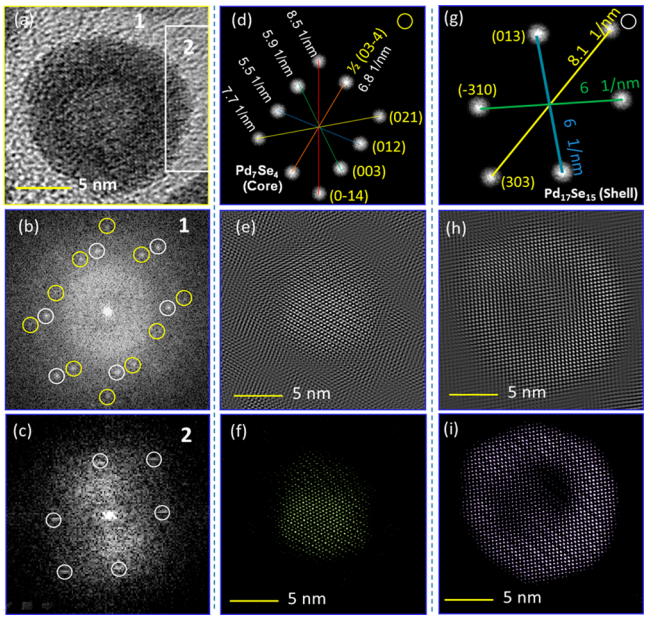

Figure 6. (a) HRTEM image of an intermediate single hollow nanostructure. (b) Selected area FFT pattern (area 1). The selected area is marked by a yellow line in (a). (c) Selected area FFT pattern taken from the edge (area 2), as marked by a white line in (a). (d) Masked FFT pattern reflecting the core only. (e) Simulated HRTEM from (d). (f) Contrast adjustment to map the core. (g) Masked FFT pattern reflected from the shell (area 2), (h) simulated HRTEM from (g), and (i) contrast adjustment mapping of the simulated HRTEM image in (h). Planes corresponding to the FFT patterns for Pd_7Se_4 and $Pd_{17}Se_{15}$ are labeled in respective panels.

6e,h) obtained from these two FFT patterns are different. From the contrasts of the images, it is clear that one reflects mostly toward a shell-like area and the other toward the core position. This implies that the hollow nanostructure is composed of multiple phases. This was more prominent when the contrasts of these two simulated HRTEM images were further tuned (Figure 6f,i). However, the simulated HRTEM image of the hollow structure presented in Figure 3i does not show any contrast difference, and a similar observation was also obtained for the final structure (Figure 6e). This further supports the suggestion that a hollow section remains inside these intermediate nanostructures. The analysis of the two FFT patterns further confirms that the inner materials resemble orthorhombic Pd_7Se_4 and that the outer materials resemble cubic $Pd_{17}Se_{15}$. From the *d*-spacings of 0.26, 0.364, 0.339, and 0.235 nm obtained from the FFT pattern in Figure 6d and from their angles, these are assigned for (021), (012), (003), and (0−14) planes of orthorhombic Pd_7Se_4. Similarly, the *d*-spacing of 0.294 nm and the angles with other planes indicate that this is an subintegral of (03−4) plane of Pd_7Se_4. On the other hand, from the FFT pattern in Figure 6g, the *d*-spacing as well as the plane angles match with (−310), (013), and (303) planes of cubic $Pd_{17}Se_{15}$ (details in Figure S7). This result regarding the phase difference is also reflected in the intermediate XRD pattern shown in Figure 5. From this, we can assume that the transformation from Pd(0) to $Pd_{17}Se_{15}$ follows a gradual conversion route, where the Pd remains more concentrated at the core and decreases toward the shell. Furthermore, we can suggest that during the selenization process, the Pd atoms diffuse out from the core to the shell, before the entire nanocrystal transforms into the single phased $Pd_{17}Se_{15}$. A schematic representation of the possible graded structure from this conversion is shown in Figure 7a, and the selenization approach for the undoped and doped Pd(0) is depicted in Figure 7b,c, respectively.

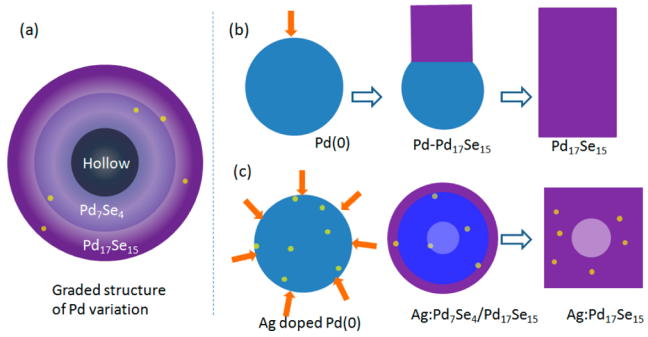

Figure 7. Schematic presentation of (a) a typical graded structure assumed to be formed during the selenization, (b) the unidirectional approach of the selenization process in the undoped nanocrystals and (c) multidirectional approach of the selenization in doped Pd(0), and the successive products.

From all these above results, we can predict that while selenization occurs all around the surface of the doped nanocrystals (Figure 7c), the Pd atoms fast diffuse out from the core to the shell, creating a void at the core. The surface Pd atoms are more exposed to the Se atoms and transformed into the final composition faster than the inner Pd atoms, which continue to diffuse outward to achieve the stable $Pd_{17}Se_{15}$ phase. This process is the Kirkendall effect, which is widely reported in the design of hollow nanostructures.[49−58] However, this effect has been observed during this study by the doping of the host Pd nanocrystals. This implies that doping, even with a low percentage (as low as 2% to the host) of dopants, can change the chemical transformation pathway and trigger the Kirkendall effect. In comparison with traditional doping, as reported in literature and discussed in the Introduction, this observation is quite unique. It directly reflects the chemical changes that are induced during the transformation of the physical shape. In our study the dopants are not introduced during the selenide growth such as in the growth doping strategy,[1,2,59,60] rather these are inserted into the metal in the zero oxidation state and are retained throughout the process. Hence, the chemical changes of the dopants are considered to be the prime factor here for driving the crystallization mechanism.

The Role of Ag Dopant in the Selenization Approach. To investigate the role of Ag, which influenced both the directional approach and the rate of selenization in the nanocrystals, we considered a particular case with only 2% Ag (with respect to Pd, see Table S1) and compared the rate for the doped and undoped cases. Figure 8 shows a schematic presentation of the reaction progress, where the amount of Se, Pd, and other reagents were kept the same and all the reactions followed the same procedure. For this case, during the transformation from Pd(0) to $Pd_{17}Se_{15}$, the transformation rate with the doped nanocrystals is observed to be ∼30 times faster than with the undoped nanocrystals. This suggests that Ag accelerates the selenization process. It is likely that Ag can form Ag-selenide faster, and with the introduction of a Se precursor, these dopant Ag atoms are converted into Ag-selenide instantaneously. Even the Ag atoms that are placed

DOI: 10.1021/jacs.5b01103
J. Am. Chem. Soc. 2015, 137, 5123−5129

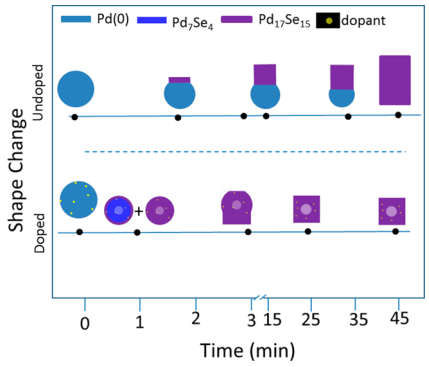

Figure 8. Plot of the time-dependent selenization progress and the shape change of doped and undoped nanocrystals. The doped nanocrystal even transformed into its final composition, $Pd_{17}Se_{15}$, within 1 min, where it took more than 30 min for the undoped nanocrystal to transform into a $Pd_{17}Se_{15}$ cuboid shape.

inside the Pd lattice can also diffuse out during the selenization process. This phenomenon is well established for the ionization of multimetallic nanostructures.[61,62] Hence, Ag-selenide nucleates first and subsequently triggers the selenization process for the whole nanocrystal. To our knowledge, this heterogeneous nucleation-induced rapid selenization of the whole host nanocrystal is specific to doping. This broadens the fundamental knowledge for the process of crystal growth in solution. Conversely, for the undoped case, the rate remains slow, and the Pd atoms have sufficient time to transform into the final stable composition of $Pd_{17}Se_{15}$. Thermodynamically, the Ag−Se bond formation is more favorable than the Pd−Se bond formation, and hence the nucleation, which is typically controlled by thermodynamic parameters, initiates first in the former case. However, the growth is kinetically controlled, and the presence of Ag−Se in the doped Pd crystal is expected to reduce the kinetic barriers for Pd−Se formation, and thus the selenization propagates faster. This rapid selenization of Pd(0) allows the transformation into $Pd_{17}Se_{15}$ via various other Pd-selenide compositions, and it also induces the Kirkendall effect.

The Intraparticle Material Transfer. Following the formation of the hollow nanostructures, thermal annealing merely reconstructed the shape from pseudospherical to cubic. To confirm this, we again considered the reaction mechanism and analyzed the solution chemistry. It was observed that the presence of TOPO in the reaction system facilitates a thermolysis-induced shape reconstruction. Under similar reaction conditions, in the control reaction in the absence of TOPO, these particles retain a hollow distorted spherical shape even after annealing (Figure S8). A similar observation was also attained for the undoped nanostructures. Hence, it can be concluded that the presence of TOPO facilitates the intraparticle material transfer that induces the shape transformation. In both cases, the exposed facets of both shapes were {100}, which we assume are the low-energy facets and are adequately capped by the TOPO. Quasi-spherical nanocrystals have several open facets, and as per the classical mechanism of formation of cube shape, the high-energy facets of the spherical particles grow and low-energy facets are created. In case of $Pd_{17}Se_{15}$, the atomic model shows that only Pd atoms are present on one atomic layer of {100} which is expected to be bound firmly by TOPO and that slowed down the growth (Figure S9). Hence, we can speculate that the high-TOPO population restricts the growth along {100} facets, while other facets grow faster and diminish. For clarity, the changes in the chemical approaches and shape transformations for both the doped and undoped cases are summarized schematically in Figure 7b,c.

CONCLUSION

In conclusion, we report on the dopant-controlled change of both the rate and directional approach of selenization in Pd(0) nanocrystals. Dopants Ag atoms are introduced at the beginning in the Pd(0) metal which nucleated the selenization process and turned the reaction to more than 30 times faster in comparison to the undoped Pd(0). This rapid rate allowed selenization to occur all around the metal Pd(0) surfaces and triggered the Kirkendall effect where the inner Pd atoms promptly diffuse outward, producing a hollow nanostructure. Consequently, the doped nanocrystals transformed into hollow cubes, and the undoped nanocrystals retained the solid cuboid structures. Hence, we can state that the heterovalent dopant-induced enhancement of the rate of selenization, the shape transformation triggered by the Kirkendall effect, and the design of new doped materials as discussed here are the new concepts of doping, and these will promote an improved understanding of the fundamental concepts of doped nanocrystals.

ASSOCIATED CONTENT

Supporting Information

Additional figures and tables supporting the results are provided. This material is available free of charge via the Internet at http://pubs.acs.org.

AUTHOR INFORMATION

Corresponding Author

*camnp@iacs.res.in.

Notes

The authors declare no competing financial interest.

ACKNOWLEDGMENTS

DST of India (project DST/SJF/CSA-01/557 2010-2011) is acknowledged for funding. N.P. and A.K.G. acknowledge DST Swarnajayanti and CSIR SPMF for a fellowship.

REFERENCES

(1) Norris, D. J.; Efros, A. L.; Erwin, S. C. *Science* **2008**, *319*, 1776.
(2) Buonsanti, R.; Milliron, D. J. *Chem. Mater.* **2013**, *25*, 1305.
(3) Pradhan, N.; Goorskey, D.; Thessing, J.; Peng, X. *J. Am. Chem. Soc.* **2005**, *127*, 17586.
(4) Zhao, Y.; Rabouw, F. T.; Puffelen, T. V.; Walree, C. A. V.; Gamelin, D. R.; de Mello Donegá, C.; Meijerink, A. *J. Am. Chem. Soc.* **2014**, *136*, 16533.
(5) Erickson, C. S.; Bradshaw, L. R.; McDowall, S.; Gilbertson, J. D.; Gamelin, D. R.; Patrick, D. L. *ACS Nano* **2014**, *8*, 3461.
(6) Santra, P. K.; Kamat, P. V. *J. Am. Chem. Soc.* **2012**, *134*, 2508.
(7) De Trizio, L.; Buonsanti, R.; Schimpf, A. M.; Llordes, A.; Gamelin, D. R.; Simonutti, R.; Milliron, D. J. *Chem. Mater.* **2013**, *25*, 3383.
(8) Mocatta, D.; Cohen, G.; Schattner, J.; Millo, O.; Rabani, E.; Banin, U. *Science* **2011**, *332*, 77.
(9) Kittilstved, K. R.; Gamelin, D. R. *J. Am. Chem. Soc.* **2005**, *127*, 5292.
(10) Chen, X.; Burda, C. *J. Am. Chem. Soc.* **2008**, *130*, 5018.
(11) Qiu, X.; Zhao, Y.; Burda, C. *Adv. Mater.* **2007**, *19*, 3995.
(12) Park, Y.; Pravitasari, A.; Raymond, J. E.; Batteas, J. D.; Son, D. H. *ACS Nano* **2013**, *7*, 10544.
(13) Kamat, P. V. *J. Phys. Chem. Lett.* **2011**, *2*, 2832.

DOI: 10.1021/jacs.5b01103
J. Am. Chem. Soc. 2015, 137, 5123−5129

(14) Viswanatha, R.; Brovelli, S.; Pandey, A.; Crooker, S. A.; Klimov, V. I. *Nano Lett.* **2011**, *11*, 4753.
(15) Pradhan, N.; Sarma, D. D. *J. Phys. Chem. Lett.* **2011**, *2*, 2818.
(16) Bhargava, R. N.; Gallagher, D.; Hong, X.; Nurmikko, A. *Phys. Rev. Lett.* **1994**, *72*, 416.
(17) Renero-Lecuna, C.; Martín-Rodríguez, R.; González, J. A.; Rodríguez, F.; Almonacid, G.; Segura, A.; Muñoz-Sanjosé, V.; Gamelin, D. R.; Valiente, R. *Chem. Mater.* **2013**, *26*, 1100.
(18) Jana, S.; Srivastava, B. B.; Jana, S.; Bose, R.; Pradhan, N. *J. Phys. Chem. Lett.* **2012**, *3*, 2535.
(19) Magana, D.; Perera, S. C.; Harter, A. G.; Dalal, N. S.; Strouse, G. F. *J. Am. Chem. Soc.* **2006**, *128*, 2931.
(20) Wang, D.; Chen, Q.; Xing, G.; Yi, J.; Rahman, B. S.; Ding, J.; Wang, J.; Wu, T. *Nano Lett.* **2012**, *12*, 3994.
(21) Pandey, A.; Brovelli, S.; Viswanatha, R.; Li, L.; Pietryga, J. M.; Klimov, V. I.; Crooker, S. A. *Nat. Nanotechnol.* **2012**, *7*, 792.
(22) Schwartz, D. A.; Norberg, N. S.; Nguyen, Q. P.; Parker, J. M.; Gamelin, D. R. *J. Am. Chem. Soc.* **2003**, *125*, 13205.
(23) Garcia, G.; Buonsanti, R.; Runnerstrom, E. L.; Mendelsberg, R. J.; Llordes, A.; Anders, A.; Richardson, T. J.; Milliron, D. J. *Nano Lett.* **2011**, *11*, 4415.
(24) Luther, J. M.; Jain, P. K.; Ewers, T.; Alivisatos, A. P. *Nat. Mater.* **2011**, *10*, 361.
(25) Comin, A.; Manna, L. *Chem. Soc. Rev.* **2014**, *43*, 3957.
(26) Kanehara, M.; Koike, H.; Yoshinaga, T.; Teranishi, T. *J. Am. Chem. Soc.* **2009**, *131*, 17736.
(27) Schimpf, A. M.; Lounis, S. D.; Runnerstrom, E. L.; Milliron, D. J.; Gamelin, D. R. *J. Am. Chem. Soc.* **2014**, *137*, 518.
(28) Srivastava, B. B.; Jana, S.; Pradhan, N. *J. Am. Chem. Soc.* **2011**, *133*, 1007.
(29) Norris, D. J.; Yao, N.; Charnock, F. T.; Kennedy, T. A. *Nano Lett.* **2001**, *1*, 3.
(30) Jana, S.; Manna, G.; Srivastava, B. B.; Pradhan, N. *Small* **2013**, *9*, 3753.
(31) Wang, F.; Han, Y.; Lim, C. S.; Lu, Y.; Wang, J.; Xu, J.; Chen, H.; Zhang, C.; Hong, M.; Liu, X. *Nature* **2010**, *463*, 1061.
(32) Yang, Y.; Jin, Y.; He, H.; Wang, Q.; Tu, Y.; Lu, H.; Ye, Z. *J. Am. Chem. Soc.* **2010**, *132*, 13381.
(33) Karan, N. S.; Sarkar, S.; Sarma, D. D.; Kundu, P.; Ravishankar, N.; Pradhan, N. *J. Am. Chem. Soc.* **2011**, *133*, 1666.
(34) Tuinenga, C.; Jasinski, J.; Iwamoto, T.; Chikan, V. *ACS Nano* **2008**, *2*, 1411.
(35) Bose, R.; Manna, G.; Pradhan, N. *J. Phys. Chem. C* **2013**, *117*, 20991.
(36) Chen, D.; Wang, Y. *Nanoscale* **2013**, *5*, 4621.
(37) Kim, S. K.; Choi, G. J.; Kim, J. H.; Hwang, C. S. *Chem. Mater.* **2008**, *20*, 3723.
(38) Zu, L.; Norris, D. J.; Kennedy, T. A.; Erwin, S. C.; Efros, A. L. *Nano Lett.* **2005**, *6*, 334.
(39) Heng, B.; Xiao, T.; Tao, W.; Hu, X.; Chen, X.; Wang, B.; Sun, D.; Tang, Y. *Cryst. Growth Des.* **2012**, *12*, 3998.
(40) De Trizio, L.; Figuerola, A.; Manna, L.; Genovese, A.; George, C.; Brescia, R.; Saghi, Z.; Simonutti, R.; Van Huis, M.; Falqui, A. *ACS Nano* **2011**, *6*, 32.
(41) Chen, J.; Wiley, B.; McLellan, J.; Xiong, Y.; Li, Z.-Y.; Xia, Y. *Nano Lett.* **2005**, *5*, 2058.
(42) Choi, B.-S.; Lee, Y. W.; Kang, S. W.; Hong, J. W.; Kim, J.; Park, I.; Han, S. W. *ACS Nano* **2012**, *6*, 5659.
(43) Vymazalová, A.; Chareev, D. A.; Kristavchuk, A. V.; Laufek, F.; Drábek, M. *Can. Mineral.* **2014**, *52*, 77.
(44) Wark, S. E.; Hsia, C.-H.; Son, D. H. *J. Am. Chem. Soc.* **2008**, *130*, 9550.
(45) Akhtar, J.; Mehmood, R. F.; Malik, M. A.; Iqbal, N.; O'Brien, P.; Raftery, J. *Chem. Commun.* **2011**, *47*, 1899.
(46) Rao, G. K.; Kumar, A.; Ahmed, J.; Singh, A. K. *Chem. Commun.* **2010**, *46*, 5954.
(47) Singh, V. V.; Rao, G. K.; Kumar, A.; Singh, A. K. *Dalt. Trans.* **2012**, *41*, 1142.
(48) Jiang, X.; Mayers, B.; Wang, Y.; Cattle, B.; Xia, Y. *Chem. Phys. Lett.* **2004**, *385*, 472.
(49) Yin, Y.; Rioux, R. M.; Erdonmez, C. K.; Hughes, S.; Somorjai, G. A.; Alivisatos, A. P. *Science* **2004**, *304*, 711.
(50) Cabot, A.; Smith, R. K.; Yin, Y.; Zheng, H.; Reinhard, B. M.; Liu, H.; Alivisatos, A. P. *ACS Nano* **2008**, *2*, 1452.
(51) Yin, Y.; Erdonmez, C. K.; Cabot, A.; Hughes, S.; Alivisatos, A. P. *Adv. Funct. Mater.* **2006**, *16*, 1389.
(52) Gao, J.; Zhang, B.; Zhang, X.; Xu, B. *Angew. Chem., Int. Ed.* **2006**, *45*, 1220.
(53) Wang, W.; Dahl, M.; Yin, Y. *Chem. Mater.* **2012**, *25*, 1179.
(54) Tang, Y.; Ouyang, M. *Nat. Mater.* **2007**, *6*, 754.
(55) Yang, Z.; Yang, N.; Yang, J.; Bergström, J.; Pileni, M.-P. *Adv. Funct. Mater.* **2015**, *25*, 891.
(56) Yang, Z.; Lisiecki, I.; Walls, M.; Pileni, M.-P. *ACS Nano* **2013**, *7*, 1342.
(57) Wang, Y.; Cai, L.; Xia, Y. *Adv. Mater.* **2005**, *17*, 473.
(58) Zhang, G.; Wang, W.; Yu, Q.; Li, X. *Chem. Mater.* **2009**, *21*, 969.
(59) Karan, N. S.; Sarma, D. D.; Kadam, R. M.; Pradhan, N. *J. Phys. Chem. Lett.* **2010**, *1*, 2863.
(60) Yang, Y.; Chen, O.; Angerhofer, A.; Cao, Y. C. *J. Am. Chem. Soc.* **2008**, *130*, 15649.
(61) Sang, W.; Zheng, T.; Wang, Y.; Li, X.; Zhao, X.; Zeng, J.; Hou, J. G. *Nano Lett.* **2014**, *14*, 6666.
(62) Gu, H.; Zheng, R.; Zhang, X.; Xu, B. *J. Am. Chem. Soc.* **2004**, *126*, 5664.

DOI: 10.1021/jacs.5b01103
J. Am. Chem. Soc. 2015, 137, 5123−5129